Cooling dynamics of a granular gas of elongated particles

Cooling dynamics of a granular gas of elongated particles

Takeichi Kanzaki[1]**, Raúl Cruz Hidalgo**[1]**, Diego Maza**[2] **and Ignacio Pagonabarraga**[3]

[1] AMADE, Departament de Física, Avenida Montilivi s/n, Universitat de Girona, E-17071 Girona, Spain
[2] Departamento de Física y Matemática Aplicada, Facultad de Ciencias, Universidad de Navarra, E-31080 Pamplona, Spain
[3] Departament de Física Fonamental, Carrer Martí i Franqués, 1, Universitat de Barcelona, E-08028 Barcelona, Spain
E-mail: tkanzakic@gmail.com, raul.cruz@udg.edu, dmaza@unav.es and ipagonabarraga@ub.edu

Abstract. The cooling dynamics of a 2D granular gas of elongated particles is analyzed. We perform simulations on the temporal evolution of soft particles, using a molecular dynamics algorithm. For weakly dissipative particles, we found a homogeneous cooling process where the overall translational kinetic energy decreases analogously to viscoelastic circular particles. In contrast, for strongly dissipative particles we observed an inhomogeneous cooling process where the diminishing of translational kinetic energy notably slows down. The rotational kinetic energy, however, always decays in agreement with Haff's prediction for the homogeneous cooling state of inelastic particles. We mainly found that the cooling kinetics of the system is controlled by the mechanisms that determine the local energy dissipation (collisions). However, we detected a strong influence of particle shape and inelasticity on the structure of the clusters which develop in the inhomogeneous cooling regimes. Our numerical outcomes suggest that strong dissipation and particle anisotropy induce the formation of ordered cluster structures that retards the relaxation to the final asymptotic regime.

Contents

1. Introduction

Granular materials are multi-particle systems involved in many industrial process and everyday life. To describe the mechanical behavior of granular materials such as sand, coffee beans, planetary rings and powders are current, challenging tasks. In the last few years, these systems have been widely examined experimentally, analytically and numerically [1, 2], and they continue to produce relevant and unexpected results [1, 2].

In particular, granular gases are dilute systems of macroscopic particles, which usually move randomly, losing energy, due to their inelastic collisions. Starting from an equilibrium homogeneous state and in the absence of any external driving, these systems evolve into a homogeneous cooling state (HCS). In such a state, the kinetic energy, $E(t)$, decreases homogeneously and the time evolution of all variables occurs only through its global temperature [3]–[5]. Haff showed that the total energy of an inelastic gas of spherical grains, characterized by a constant restitution coefficient, evolves in time as a power law, $E(t) = 1/(1 + t/\tau)^2$, where τ is a characteristic time [6]. Very recently, Haff's law has been experimentally corroborated in systems of magnetized latex particles [7].

For any given inelasticity and above a certain system size, HCS becomes unstable and the system subsequently evolves into an inhomogeneous state where the cooling process slows down and decays as $E(t) = 1/(1 + t/\tau_h)$, independently of inelasticity [8, 9]. In this regime the collective motions of particles and vorticity determine the cooling of the gas, and large inhomogeneities in density are observed [8, 10, 11]. Hence, large clusters of particles develop, grow and interact due to the energy lost in collisions [8, 10, 11]. While for an infinite system this regime has been argued to correspond to the asymptotic free cooling evolution of a fluid of inelastic hard spheres, for any finite system clusters eventually become of the order of the system size; in this regime the kinetic energy decays as that in the HCS [7, 8, 12, 13]. These dynamical regimes, predicted theoretically, have also been validated numerically for hard discs and spheres with constant restitution coefficient [1, 2]; in particular, Haff's law in the HCS [8], the algebraic decay in the hydrodynamic regime [9] and the regime where cluster sizes become of the order of the system size [8] have been validated.

There is experimental evidence that in some materials the restitution coefficient is not constant and that it rather depends on the relative velocity of the colliding grains. Moreover, there have been a number of theoretical studies which have analyzed in more

detail the particle–particle interaction during the collision and how inelasticity emerges from such interactions [14]–[16]. For soft grains in which the repulsion force depends linearly on deformation, a constant restitution coefficient can be recovered [17, 18]. A more realistic account of particle deformation implements a Hertzian contact [17, 19], where the nonlinear elastic repulsive force leads to an algebraic decay of the kinetic energy during HCS which deviates from Haff's law, $E(t)/E_0 = 1/(1 + t/t_0)^{5/3}$ [15, 20]. The implications of variable restitution coefficients in the instability of HCS and the subsequent inhomogeneous cooling regime have been addressed for viscoelastic spheres, where homogeneous cooling becomes the asymptotic state after a long transient controlled by inhomogeneous large clusters [21].

In the past, it was also shown that particle roughness leads to correlations between translational and rotational degrees of freedom and their corresponding kinetic energies [12], [22]–[24]. In general, both translational and rotational kinetic energies decay following Haff's law but differ from each other due to the breakdown of energy equipartition leading to correlations between translational and rotational kinetic energies; such correlations have been quantified for agitated spherical rough spheres [25, 26]. However, less is known about the freely cooling evolution of anisotropic particles [27, 28], although recently there has been increasing interest in the dynamics of rod-shaped grains [29]–[33]. For example, in vibrated systems the particle anisotropy leads to net displacements and propulsion [34]. Such types of collective features favor clusters and other types of patterns, reminiscent of those observed in a system of self-propelled elongated particles in model systems [35] motivated from biological materials [36, 37].

In the present work, we investigate the free cooling process of a granular gas of elongated viscoelastic particles. In the next sections, we analyze the role of inelasticity and particle shape in the overall kinetic processes. Moreover, the structures and patterns which develop as the system cools down are studied in detail. This paper is organized as follows: first, the specific model is described in section 2. Subsequently, in section 3 we discuss the kinetics of freely evolving grains and clarify the main features that grain shape has in the clusters that the grains develop. We conclude in section 4 with a summary of the main results and their implications.

2. The model

We consider a system of $2D$ irregular convex polygons, which are generated by a random Voronoi tessellation. The latter allows us to generate particles with variable degrees of irregularity systematically [38]. Accordingly, the particle shape distribution is characterized by a single parameter $0 < a < 1$. The extreme value $a = 0$ corresponds to a regular distribution of rectangles with sides $S_1 = 1$ and $S_2 = d$, where $d > 1$ defines the grain aspect ratio.

Following our description, a system composed of N particles, of mass m_i and moment of inertia M_i, move according to Newton's equations of motion:

$$m_i \ddot{\vec{r}}_i = \sum_{j=1}^{N} \vec{F}_{ij}, \tag{1}$$

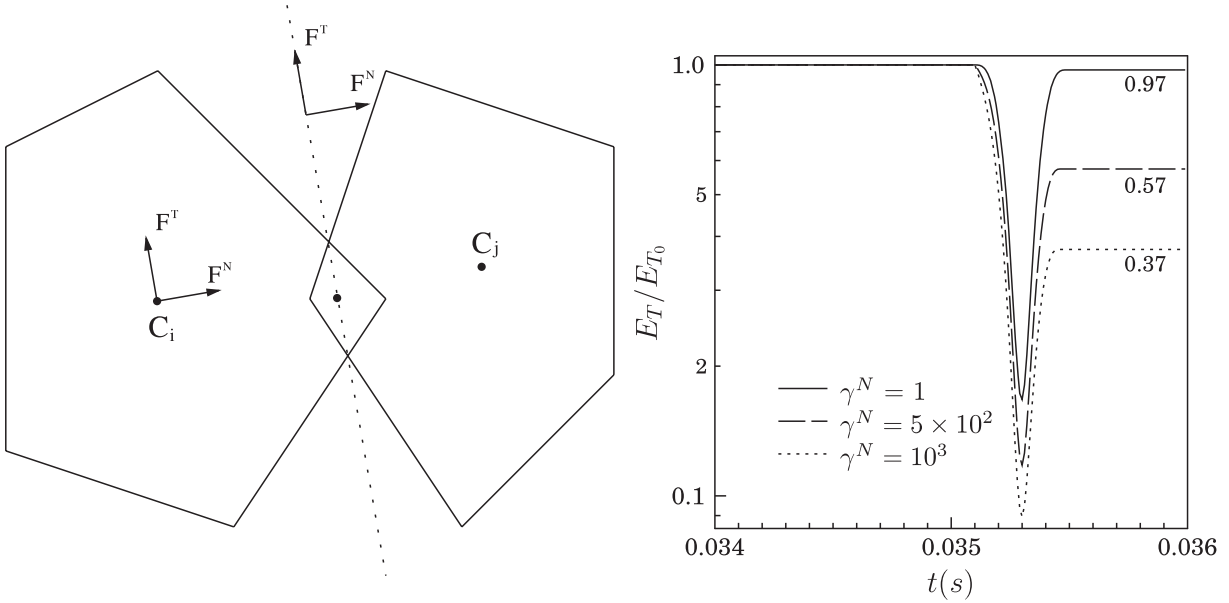$$M_i \ddot{\theta}_i = \sum_{j=1}^{N} L_{ij}, \tag{2}$$

Figure 1. In (a) a sketch of two interacting particles is presented. The force between two particles is proportional to the overlap area. The force is applied at the middle point of the line connecting the intersection points of the particles. In (b) we show the total kinetic energy loss due to the collision of two particles, expressed as the ratio of the total energy after and before the collision ($E_{\mathrm{T}}/E_{\mathrm{T_0}}$). The total energy is computed as the sum of kinetic and rotational energies. The values shown here correspond to the maximum velocity experienced by the particles.

in terms of the particle position $\vec{r_i}$ and orientation θ_i. $\vec{F}_{ij}$ corresponds to the force exerted by particle j on particle i and L_{ij} the torque related to the force $\vec{F}_{ij}$, which points in the direction perpendicular to the plane in which the particles displace. The total force and the total torque acting on particle i are given as sums of the pair-wise interaction of particle i with its contacting neighbors. Accordingly, the grains' trajectories will be determined once we identify the nature of the collisional forces.

When two particles come in contact they deform inelastically. Rather than describing the actual grain deformations, we keep the shape of the particles and allow them to overlap and determine the particle forces in terms of the overlapping area [38]–[42]. Accordingly, the total force between the two grains can be decomposed:

$$\vec{F}_{ij} = F_{ij}^{\mathrm{N}} \cdot \vec{n} + F_{ij}^{\mathrm{T}} \cdot \vec{t} \tag{3}$$

into components normal, F_{ij}^{N}, and tangential, F_{ij}^{T}, to the interface defined by the contact points of the two particles when they overlap. We introduce the normal, $\vec{n}$, and tangential, $\vec{t}$, vectors to the common interface, which is depicted in figure 1(a). The force is applied at the middle point of the common interface. Although the center of mass of the overlapping area could have been chosen as the relevant position [42], no qualitative changes have been appreciated in tests performed as far as the results described subsequently are concerned.

The normal component contains an elastic contribution, proportional to the pair overlap area, A_{ij}, and a dissipative contribution:

$$F_{ij}^{\mathrm{N}} = -k_n A_{ij} - m_{ij}^{\mathrm{eff}} \cdot \gamma^{\mathrm{N}} \cdot v_{ij,\mathrm{rel}}^{\mathrm{N}}, \tag{4}$$

where k_n is the Young modulus, γ^{N} is the damping coefficient in the normal direction, $m_{ij}^{\mathrm{eff}} = (m_i \cdot m_j/m_i + m_j)$ is the relative mass of the colliding pair and $\vec{v}_{ij,\mathrm{rel}}^{\mathrm{N}} = (\vec{v}_j - \vec{v}_i) \cdot \hat{n}$ stands for the normal component of their relative velocity. In general, for regular particles it is possible to derive analytic expressions for the overlap area as a function of the separation between the particle's center of mass. For particles of irregular shape, however, it is computed numerically [38]–[42].

The tangential component of the interaction force is characterized also by an elastic and a dissipative contribution, and obeys the Coulomb constraint, $F_{ij}^{\mathrm{T}} \leqslant \mu|F_{ij}^{\mathrm{N}}|$, where μ stands for the static friction coefficient. Accordingly, we write

$$F_{ij}^{\mathrm{T}} = -\min(-k_t\xi_{ij} - m_{ij}^{\mathrm{eff}} \cdot \gamma^{\mathrm{T}} \cdot |v_{ij,\mathrm{rel}}^{\mathrm{T}}|, \mu|F_{ij}^{\mathrm{N}}|), \tag{5}$$

where γ^{T} is the damping coefficient in the tangential direction and $\vec{v}_{ij,\mathrm{rel}}^{\mathrm{T}} = (\vec{v}_j - \vec{v}_i) \cdot \hat{t}$ corresponds to the tangential component of their relative velocity. The elastic force is now characterized by ξ_{ij}, the elastic elongation associated with the overlapping pair. It behaves as a Cundall spring [43]:

$$\frac{\mathrm{d}\xi_{ij}(t)}{\mathrm{d}t} = v_{ij,\mathrm{rel}}^{\mathrm{T}}, \tag{6}$$

which evolves as long as there is an overlap between the two particles.

The equations of motion, equations (1) and (2), are integrated using a fifth-order predictor–corrector algorithm with a numerical error proportional to $(\Delta t)^6$ [44], while the kinematic tangential relative displacement, equation (6), is updated using Euler's algorithm. In the simulations, we have used the parameters $k_t/k_n = 0.1$, $\gamma^{\mathrm{N}}/\gamma^{\mathrm{T}} = 3$, $k_n = 4 \times 10^2$ N m and $\mu = 0.25$, introduced in previous works [41, 42]. For this range of parameters we have set a time step $\mathrm{d}t = 10^{-6}$ s. The damping coefficients γ^{N} and γ^{T} quantify the inelasticity of the collision. In order to address their impact on the evolution of anisotropic grains, we have varied them. To understand their relationship with the energy lost in a collision, we have analyzed the interaction between a pair of rectangles. In figure 1(b) we display the behavior of the total kinetic energy, E_{T}, during one collision. For convenience, the values are rescaled to the total kinetic energy just before the collision starts, $E_{\mathrm{T_0}}$. The data correspond to several damping coefficients γ^{N}, which quantifies the variation and the relevant range of dissipation. The numerical values of the corresponding effective restitution coefficients are also shown. In general, the total energy lost strongly depends on the initial particles' relative velocity. Consequently, to identify the effective velocity-dependent restitution coefficient is not very obvious. The values of the damping coefficient displayed range from particles which loose a rather small amount of kinetic energy up to particles where around 70% of the pair's incoming relative kinetic energy is lost in one collision. The data shown correspond to particles with a relative impact velocity of 1 m s^{-1}, which is the highest value experienced by the particles in the present numerical studies.

In the next sections, we focus on rectangles with variable aspect ratio, d. For the rectangles, when two vertices overlap with the same side, no special care is necessary as long as the parameters used always warrant that the maximum overlap is much smaller than the particle size. In the very unlikely situation where two vertices of one particle overlap with a pair of vertices of a second particle, leading to full face-to-face interaction, the contact surface is defined by the two middle points between the corresponding closest
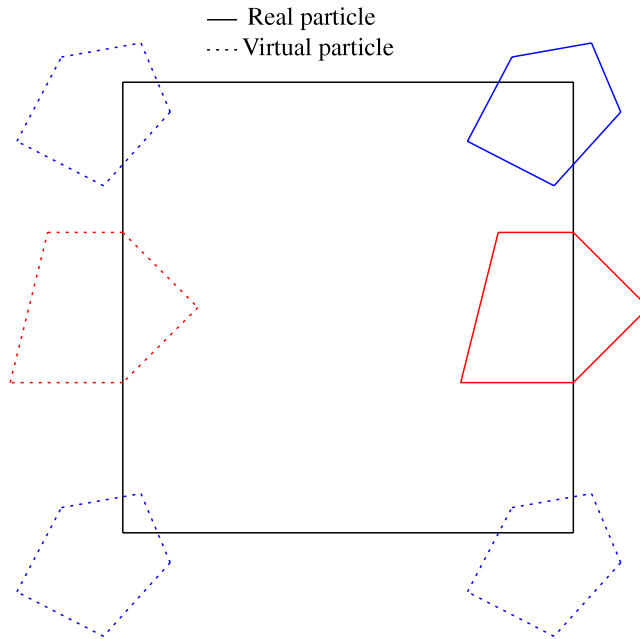
Figure 2. When a particle starts to leaves the system, a virtual particle is *created* on the opposite side (red particles). For the particular case that the particle leaves the box from a corner then a virtual particle is *created* at all the other corners (blue particles).

pair of vertices. The other steps of the procedure remain unchanged. Systems of irregular particles characterized by a parameter $(1/4 \leq a \leq 1/2)$ (data not shown) were also explored, without observing any relevant differences from the results we will analyze below.

Boundary conditions

The simulations are carried out in a square box of size L and a fixed number of grains, N, at a prescribed area fraction, ν. In order to minimize finite size effects, we have used periodic boundary conditions. Due to the general shape of the grains, whenever a particle leaves one side of the box, we need to replicate it on the opposite side. Accordingly, we generate a list of *virtual particles* which include all particles that have at least one vertex out of the system. As soon as a particle starts leaving the system, it is added to the list of *virtual particles*. When the center of mass of the particle crosses one of the system's boundaries, then the position of the reference particle is updated following the standard procedure. Such a change alters the status of the reference particle and the virtual ones, which is updated appropriately in the *virtual particle* list. For consistency in the case the particle goes out through a corner, three virtual particles are created, as illustrated in figure 2. The virtual particles are regarded as standard particles when computing inter-particle forces. Note that the force computed for a virtual particle is applied to the corresponding *real* particle the *virtual* particle is linked to. Also the change in position of the real particle leads to the corresponding change of the virtual particles linked to it.

3. Freely evolving anisotropic grains

We have numerically studied the free cooling kinetics of a dilute system of $N = 3000$ polygons at area fraction $\nu = 0.07$ confined within a square box. Initially, the particles are homogeneously distributed and their translational and rotational velocities follow Gaussian distributions. In order to avoid memory effects from the initial conditions, we allow the system to execute a few collisions before starting to analyze the particles' temporal evolution, which we follow until the total mean translational and rotational kinetic energies have decayed several orders of magnitude. All data shown correspond to averages over at least five different initial configurations.

In figures 3 and 4 we display snapshots of the density and velocity fields for rectangular grains with aspect ratio $d = 5$. We have explored the system's behavior for two extreme damping coefficients (used in figure 1(b)) to quantify the inelasticity of typical collisions. In both cases we can distinguish an initial homogeneous decay, which corresponds to HCS. This state is unstable and the granular gas develops density inhomogeneities leading to cluster formation. Since eventually the decay in the grains' velocity will reduce the inelasticity lost in the collisions, we expect a homogeneous asymptotic behavior analogous to the one put forward for viscoelastic isotropic grains [15, 21].

The behavior of the granular gas in the inhomogeneous regime shows a clear dependence on the damping coefficient, γ^N. For weakly dissipative particles, $\gamma^N = 1 \text{ s}^{-1}$ (see figure 3), one can appreciate the smooth development of a velocity field leading to the formation of clusters which coalesce and merge into large structures (see figure 3(b)). At longer times, however, these large clusters show a tendency to break, avoiding the development of the *clustering instability* (see figure 3(c)), in agreement with the predictions for viscoelastic grains [21, 45]. In contrast, highly dissipative grains, with $\gamma^N = 10^3 \text{ s}^{-1}$, develop marked clusters of smaller sizes much faster, as can be appreciated in figure 4. Such clusters are correlated with the rapid development of complex vortex structures in the grains' velocity field. These well-defined small clusters tend to coalesce at larger times, although the overall process of large cluster development is severely slowed down when compared to the evolution of weakly dissipative clusters. Increasing the particle anisotropy (data not shown) enhances this distinct evolution with the particle energy dissipation. In the past, a similar trend has been observed for rough spheres, where it has been shown that energy transferred into rotational degrees of freedom delays cluster development [26].

We have quantified the temporal evolution of freely evolving gases of rectangular grains by monitoring the mean translational and rotational kinetic energy of the system, usually referred to as granular temperatures. Figure 5 displays the decay of the translational kinetic energy, $E(t)$, of a granular gas for weak and strong dissipative rectangular grains with aspect ratio $d = 5$. After a short transient, $t > 0.1$ s the decay is algebraic, in agreement with the analytic predictions for the homogeneous cooling state of hard and viscoelastic grains.

Since the dissipation in these systems is proportional to the relative velocity difference and the restitution force is a nonlinear function of the overlapping area (see equation (4)), one can expect the system evolves analogously to a gas of hard viscoelastic grains [15]. We have verified that this is consistent with the results obtained for weakly dissipative grains. The algebraic decay depicted in figure 5(a) is characterized by the same exponent,
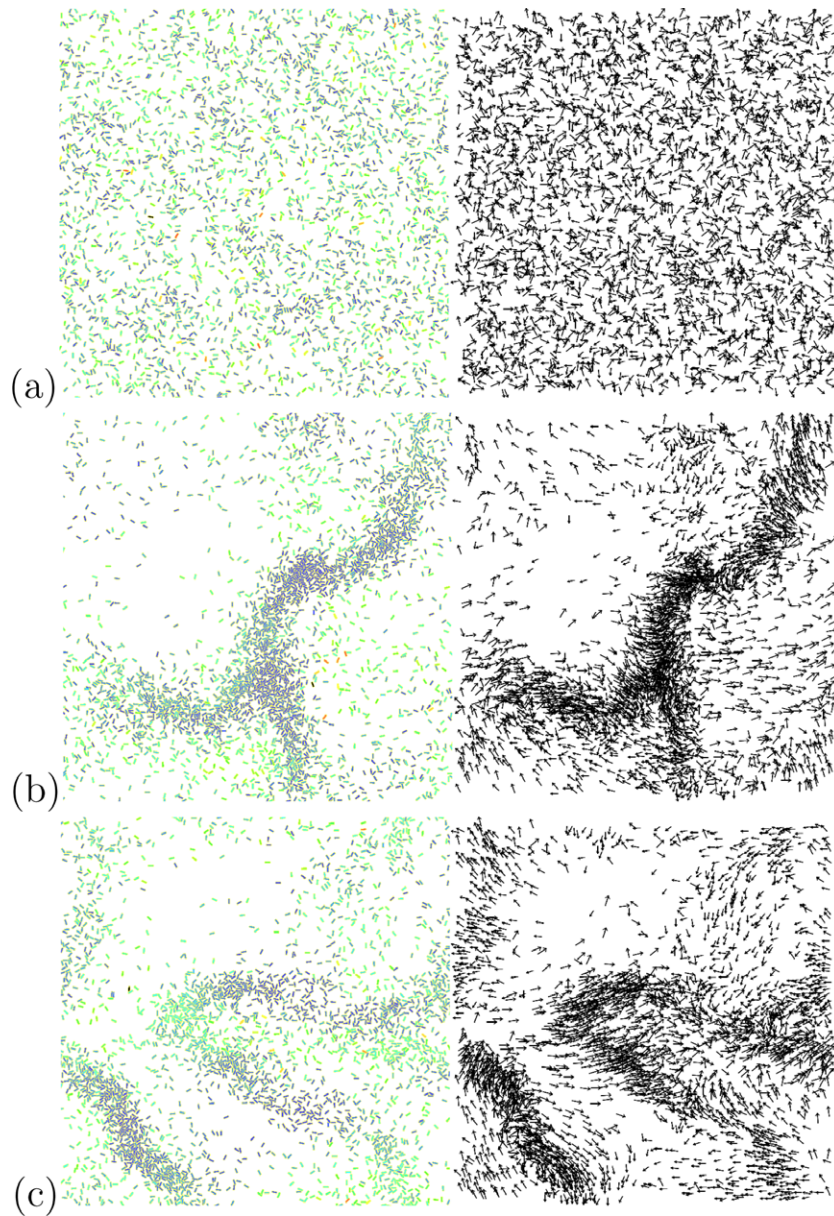
Figure 3. Spatial evolution of a system with elongated particles $d = 5$ and a damping coefficient of $\gamma^N = 1 \text{ s}^{-1}$. The first column shows the screenshots of the system, while the second illustrates the velocity fields. The lighter the particles the faster they are. Pictures at $t = 10$ s (a), $t = 100$ s (b) and $t = 200$ s (c) are presented.

$\beta = -\frac{5}{3}$, analytically predicted for viscoelastic grains [15]. However, this is not the case for highly dissipative grains, which cool down slower, with a characteristically smaller exponent, $\beta \approx -1.2$, in the algebraically decaying regime. It is important to remark that the limitations of the numerical scheme used prevented us from performing calculations with higher dissipative systems, to reach the hydrodynamic algebraic decay $E(t) \sim t^{-1}$ limit [9].
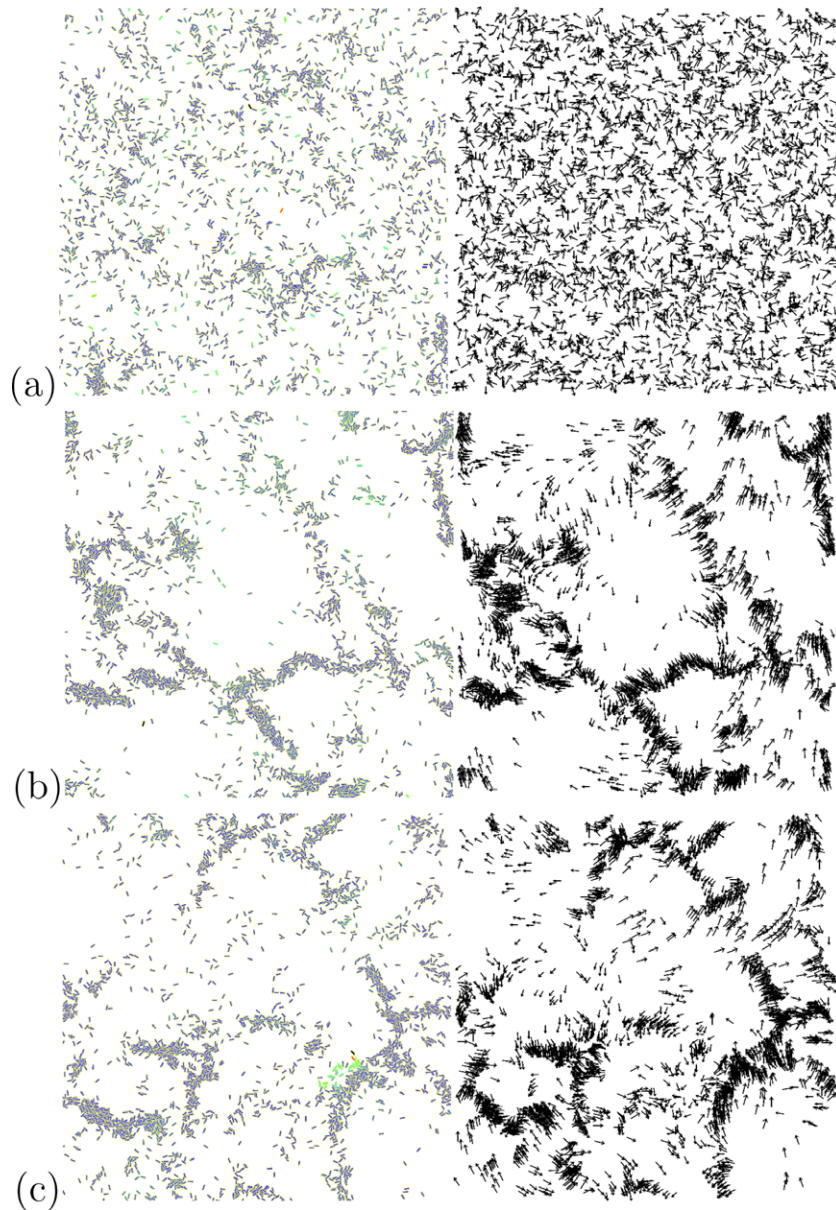
Figure 4. Spatial evolution of a system with elongated particles $d = 5$ and a damping coefficient of $\gamma^{\mathrm{N}} = 10^3$ s^{-1}. The first column shows the screenshots of the system, while the second illustrates the velocity fields. The lighter the particles the faster they are. Pictures at $t = 10s$ (a), $t = 100$ s (b) and $t = 200$ s (c) are presented.

On the other hand, for weakly dissipative systems, the decay of the translation kinetic energy also slows down at longer times. This can be attributed to the development of stronger velocity correlations. Nevertheless, the narrow time regime (system size effects) does not allow us to quantify the algebraic dependence characteristic of the hydrodynamic regime, $E(t) \sim t^{-1}$ [9]. In contrast, the faster decay ($t^{-5/3}$), which can be attributed to the dominance of large clusters, is quickly recovered. Larger system sizes will be required
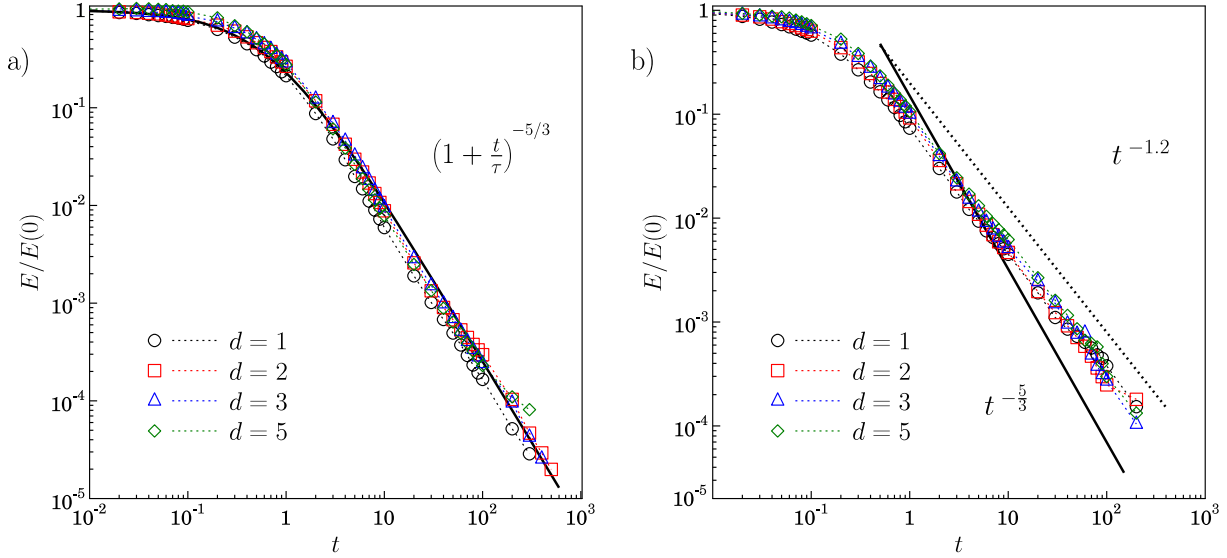
Figure 5. Evolution of the translational kinetic energy of the system in time. Particles with several aspect ratios from $d = 1$ to 5 are studied. Results for two very extreme damping values are shown, (a) $\gamma^{\mathrm{N}} = 1$ s^{-1} and (b) $\gamma^{\mathrm{N}} = 10^3$ s^{-1}. For comparison the analytical prediction for a system of viscoelastic circles as well as our best fit for the inhomogeneous cooling process are shown as lines.

to identify the relevance of the intermediate regimes before reaching the asymptotic state. For highly dissipative grains the smaller exponent, observed from very short times, may suggest an earlier departure from HCS. In this case, the interplay of cluster formation and break up with the development of large clusters and their impact on the overall kinetic energy decay also remains to be clarified. Nevertheless, figures 5(a) and (b) clearly indicate that neither the dissipation nor the shape significantly modify the functional dependence and the characteristic timescales in which the systems cool down. Moreover, analogous results (data not shown) are obtained for irregular particles with ($1/4 \leq a \leq 1/2$).

Figure 6 shows the decay of the rotational kinetic energy. After a short transient, for $t > 1$ s, we observe an algebraic decay characterized by an exponent -2 regardless of particle shape and inelasticity. This exponent, in agreement with Haff's law, can be understood assuming weak rotational–translational correlations. The latter can be traced back to the fact that, above the Coulomb threshold, both the elastic and dissipative contributions of the tangential force are linear functions of the lateral displacement and relative velocity, respectively (see equation (5)). The deviations observed in $E(t)$ at longer times are much weaker for rotational kinetic energy, suggesting that rotations are much less sensitive to the development of spatial inhomogeneities. The different behavior in the decay of rotational and translational kinetic energy indicates a lack of energy equipartition during the whole cooling process of the anisotropic grains, both in the homogeneous and inhomogeneous regimes.

During the cooling process the velocity statistics was also examined (see figures 7(a) and (b)). Starting from a Maxwellian speed distribution, the particle velocity distribution evolves with a scale characterized by the mean translational kinetic energy. For weakly dissipative particles, which cool down more uniformly over a wide range of times, it is
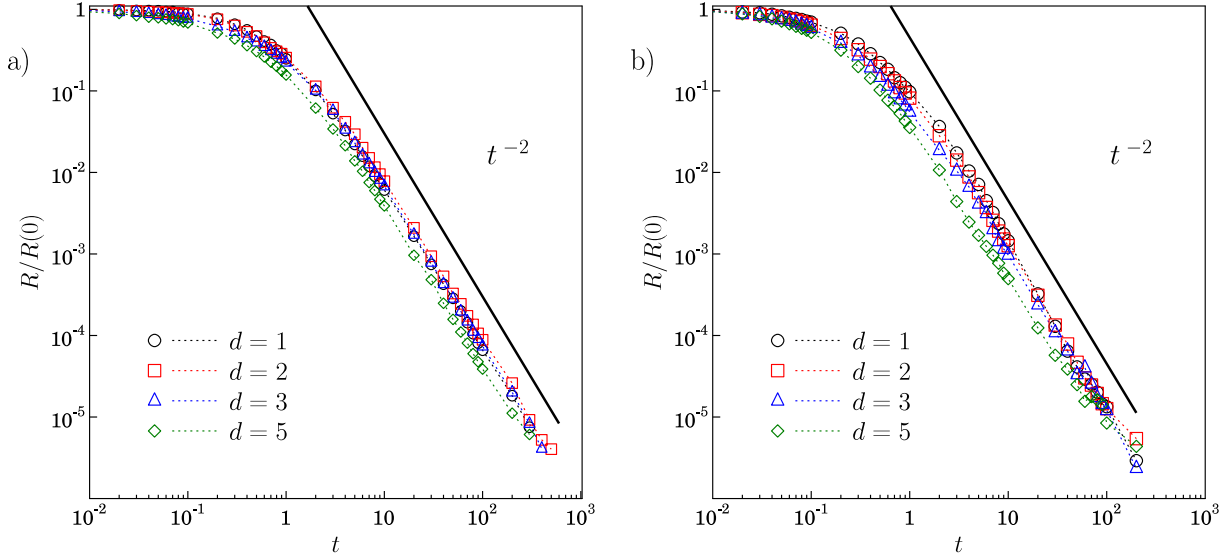
Figure 6. Evolution of the rotational energy of the system in time. Particles with several aspect ratios from $d = 1$ up to 5 are studied. Results for two very extreme damping values are shown: (a) $\gamma^{N} = 1$ s^{-1} and (b) $\gamma^{N} = 10^{3}$ s^{-1}. For comparison Haff's analytical prediction t^{-2} is also shown.

reasonable to expect that all the temporal dependence enters through the translational temperature and we can then identify a dynamic scaling regime where the scaled velocity distribution becomes stationary. Such a picture is consistent with the results shown in figure 7(a), where we show the scaled speed distribution, $P(c)$ ($c = v/\bar{v}$), at the initial and final times. Regardless of the particle anisotropy, the distribution shape remains close to a Maxwellian. For highly dissipative grains, larger fluctuations are observed, although the shape also remains close to a Maxwellian. In this case, one can argue that such a behavior arises as a result of the presence of independently evolving clusters. Finite size limitations prevents us from analyzing the tails of the distributions, where deviations from the Maxwellian behavior may develop and become good indicators of the different features of weak and strong dissipative granular gases.

To gain insight into the role of particle anisotropy on the collective features of freely evolving granular gases, we have analyzed the structure of the clusters which the system spontaneously develops. In the simulations, two particles are regarded as part of the same cluster if there is any contact between them, i.e. when the inter-particle overlap area is larger than 10^{-6}. We have first considered the radial distribution function of connected particles $G(r)$ within a given cluster:

$$G(r) = \left\langle \frac{N(r + \delta r)}{2\pi r \delta r \rho} \right\rangle, \tag{7}$$

where $\rho = N_{T}/A$ is the average number of rods per unit of area measured by counting the total number of rods N_{T} whose center of mass lies in the analyzed area A. $N(r + \delta r)$ accounts for the number of particles, within the cluster, with their center of masses at a distance r within a differential of area $\delta S = 2\pi r \delta r$. The value of $G(r)$ corresponds to a mean value obtained over the whole system.
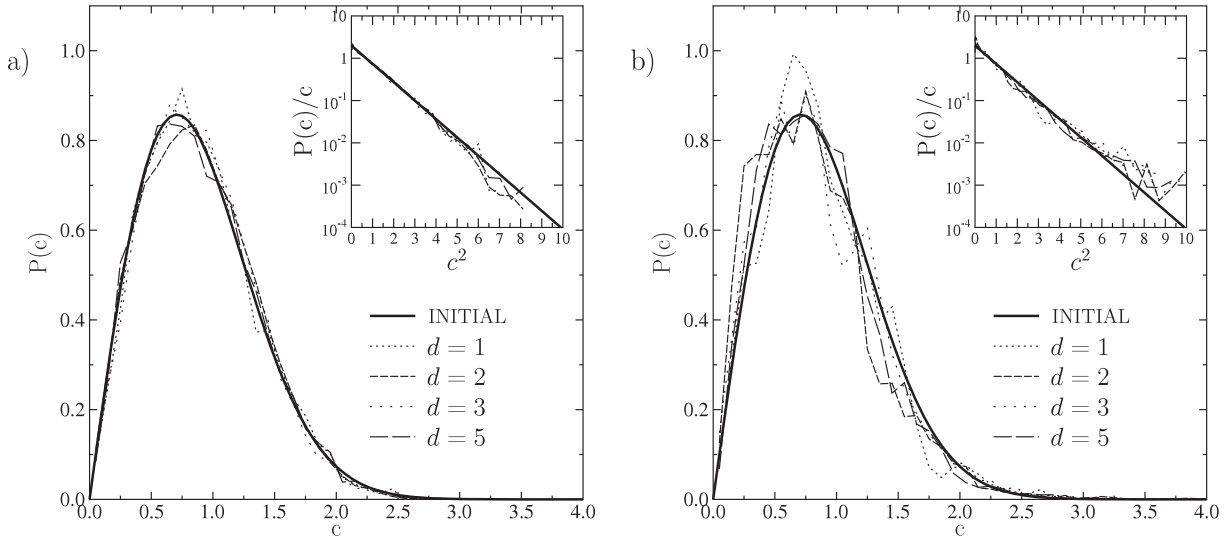
Figure 7. Scaled speed distribution of several particle shapes, ranging from $d = 1$ to 5. In all cases, the data correspond to very late times; for comparison, the initial speed distribution is also shown. (a) Weak dissipative particles, $\gamma = 1$ and (b) strong dissipative particles, $\gamma = 10^3$. The insets show the tails of the velocity distribution functions.

In figure 8, the radial distribution function of connected particles, $G(r)$, is illustrated for particles with different damping coefficients and a variety of aspect ratios. At short distances, weakly dissipative grains display weak, short range correlations characterized by the particle's longest side, clearly visible in figure 8(a). One can appreciate a correlation hole close to contact and subsequently the radial distribution function develops a smooth peak whose relative height decreases as the particle anisotropy increases. For strongly dissipative particles the short range structure is markedly different, as shown in figure 8(b). The inelasticity induces strong short range structures which correspond to the different structures in which the particles can pack locally, depending on their aspect ratio. The drawings in the figure indicate some of the structures where one can find particles either perfectly aligned parallel to each other along their long faces, or perpendicular to each other, alternating long and short faces. This packing gives rise to clearly marked peaks, whose positions change with the aspect ratio, d. The relative height of the peaks also decrease with particle anisotropy, but in all cases their heights are larger than the corresponding particle anisotropies with a smaller damping coefficient. This tendency to more marked close-packed structures arises as a combined effect of dissipation and alignment-induced packing associated with the particle's shape. The insets of figure 8 display the long distance decay of the radial distribution function. The particle dissipation gives rise to larger values of the radial distribution function at contact, but in both cases, and for all the aspect ratios analyzed, we observe a long range decay, characteristic of the development of long range clusters and structures. Such long range structures have been observed in agitated isotropic grains as a result of long range hydrodynamic correlations due to the lack of detailed balance in these out-of-equilibrium systems [46].

Further information on the local structure of rod alignment is obtained from the radial orientational distribution of connected particles within a given cluster, $Q(r)$, which can
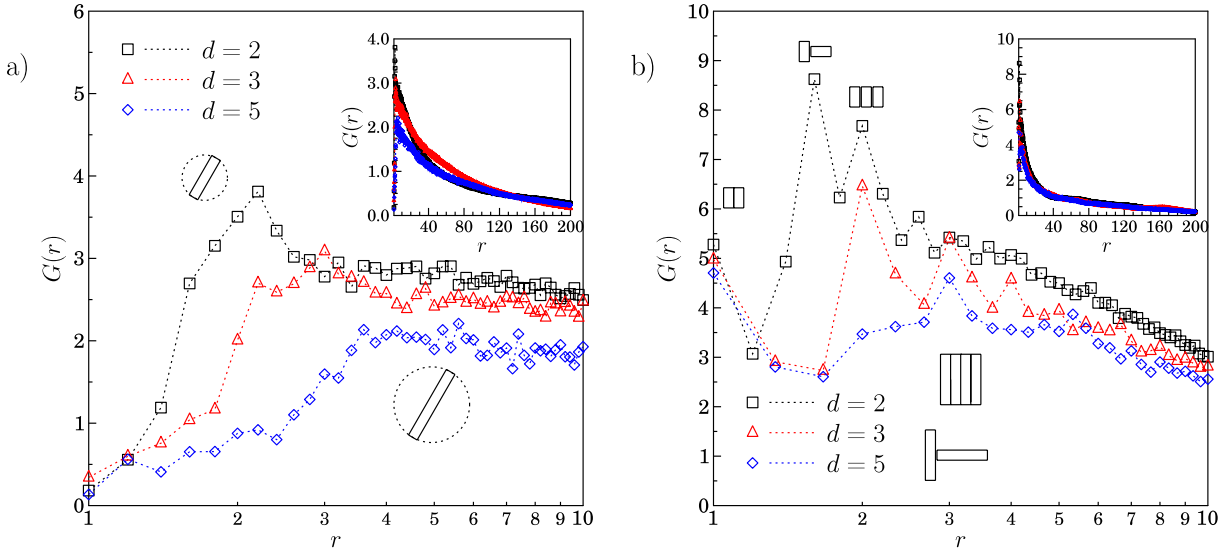
Figure 8. Radial distribution function of connected particles obtained for a system of particles with aspect ratios from $d = 2$ to 5. Results for two very extreme damping values are shown: (a) $\gamma^N = 1$ s^{-1} and (b) $\gamma^N = 10^3$ s^{-1}. In both cases the particle alignment corresponding to a few relevant peaks in the radial distribution function is drawn.

be defined as

$$Q(r) = \langle Q_{ij} \rangle \qquad Q_{ij} = \cos\left(2(\theta_i - \theta_j)\right)\delta(\mathbf{r}_{ij} - r) \tag{8}$$

where θ_i and θ_j are the angular orientation of particles i and its connected neighbor j, at a distance r_{ij}. This distribution function provides quantitative information on the local structure of the clusters because configurations where the two particles are perpendicular to each other contribute -1, while particles aligned along their long faces or along their short faces contribute 1.

In figure 9(a), the $Q(r)$ numerical data clearly indicate that weakly dissipative systems do not show significant structure. There is a peak at contact ($r = 1$), because at this shortest distance only perfectly aligned particles along their long faces can contribute. At larger distances a small dip indicates a small preference at these intermediate distances to observed perpendicularly aligned particles. But, overall, it is the relaxation from the completely aligned structure at contact which dominates $Q(r)$. In contrast, figure 9(b) shows that, after the decay of the compact structure at contact, a series of maxima (parallel alignment) and minima (perpendicular alignment) develop at intermediate distances corresponding to the high tendency of these dissipative particles to align in close-packed structures. The radial orientation distribution function shows a faster decay than the radial distribution function, suggesting that angular correlations are short range.

Finally, in figure 10 we show the local nematic order parameter for the freely evolving gas, $S(t)$, defined as

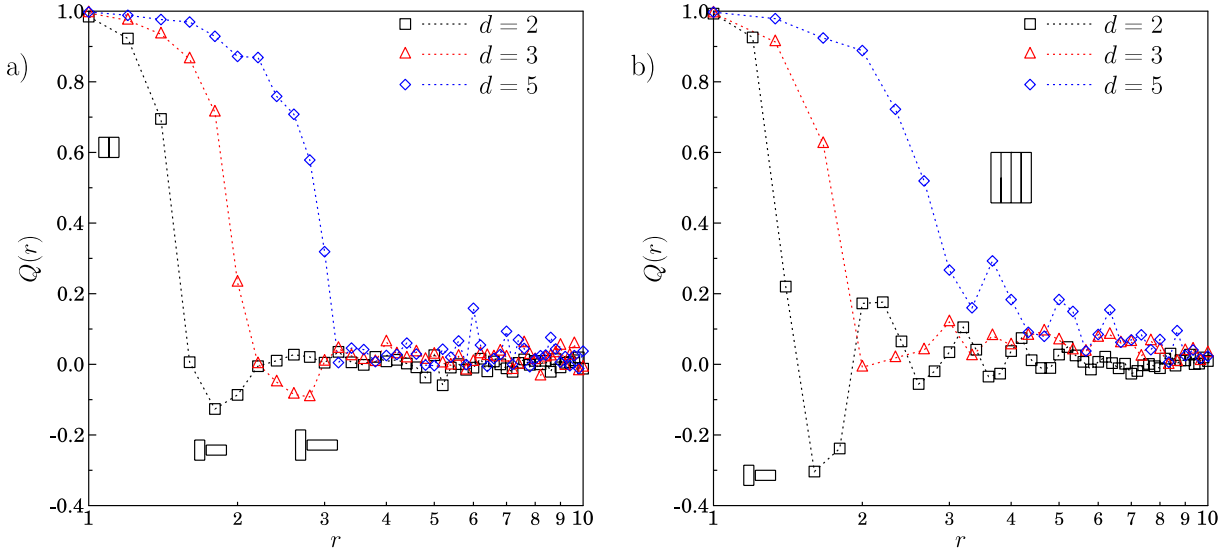$$S(t) = \frac{1}{N} \sum_i^N \frac{1}{N_c} \sum_j^{N_c} Q_{ij} \tag{9}$$

Figure 9. Radial orientation distribution functions of connected particles, $Q(r)$, as defined in equation (8) for a system of particles with aspect ratios from $d = 2$ to 5. Results for two very extreme damping values are shown: (a) $\gamma^{\mathrm{N}} = 1$ s^{-1} and (b) $\gamma^{\mathrm{N}} = 10^3$ s^{-1}. In both cases the particle alignment corresponding to a few relevant peaks in the radial orientation distribution function is drawn.

We restrict the sum of the orientational function, introduced in equation (8), to the particles which are in contact with a reference particle i. N_c is the number of particles that are in contact with i. $S(t)$ naturally captures the local angular correlation, and it runs from $S(t) = 1$, representing the maximum local correlation, to $S(t) = 0$, which corresponds to a locally disordered system. Figure 10 clearly indicates that particle anisotropy induces local nematicity in the clusters of particles, even at very early stages for highly dissipative particles. The local ordering into a nematic structure grows with particle anisotropy. For weakly dissipative particles, however, no local angular correlation is found, as shown in the inset of figure 10. For these particles the clusters gather particles which avoid overlapping each other but without any significant local angular correlation.

4. Discussion

In summary, we have examined the cooling dynamics of a 2D granular gas of elongated grains. For weakly dissipative particles, we have found that the mean kinetic energy decreases asymptotically as $E(t)/E_0 = 1/(1 + t/t_o)^{5/3}$, in agreement with the Brilliantov and Pöschel predictions for the homogeneous cooling state regimen (HCS) of viscoelastic particles [15, 20]. A higher dissipation induces an inhomogeneous cooling process and the energy vanishes as $E(t)/E_0 \sim t^{-1.2}$. The rotational energy, however, always decays as $R(t)/R_0 \sim t^{-2}$, which is in agreement with Haff's prediction for the HCS of inelastic particles. The lack of energy equipartition is kept even during the inhomogeneous cooling process where strong inhomogeneities in the velocity field are present.

We have also observed a strong influence of particle shape and inelasticity on the structure of the clusters which develop in the inhomogeneous cooling regimes. The
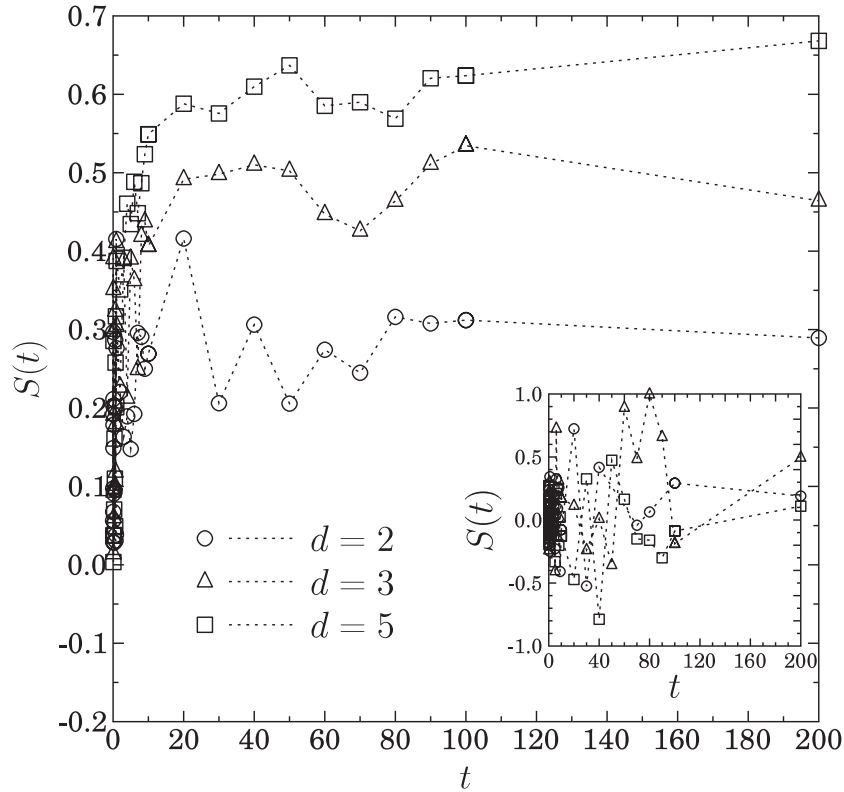
Figure 10. Nematic parameter at contact, $S(t)$. Results for $\gamma = 10^3$ s^{-1} and three different anisotropies are depicted. The inset shows the corresponding behavior for weakly dissipative particles, $\gamma = 1$ s^{-1}.

combined analysis of the radial distribution function, $G(r)$, the angular correlation, $Q(r)$, and the local nematic order parameter, $S(t)$, clarify the cluster structure. Highly dissipative grains show a marked tendency to form ordered clusters with strong local angular correlations. Therefore, the system is nematogenic in this cooling process, and one can expect that the observed clusters display a significant nematic order. The latter, which increases with particle elongation, is very closely related to the typical face-to-face interaction. The relevance of the interplay between particle shape and inelasticity has been clearly appreciated by analyzing the structures of weakly dissipative grains, where the local nematicity is essentially absent and the density inhomogeneities are statistically much more isotropic. Our numerical outcomes suggest that the strong dissipation and the particle anisotropy induce the formation of ordered cluster structures and velocity vortices, which notably slow down the cooling process and retard the appearance of large clusters which break and reform. Increasing the particle anisotropy enhances this distinct evolution as a function of the particle energy dissipation. This behavior can be attributed to the detailed interaction between ordered clusters of particles, where rotational degrees of freedom play a relevant role. The break up of large clusters of elongated particles as a result of their collisions leads to the formation of smaller clusters, promoting a faster decay of the rotational kinetic energy. Such smaller clusters of ordered particles in turn delay the development of the inhomogeneous cooling regime. Understanding the impact

of these strong correlations in agitated systems where energy is supplied continuously constitutes an interesting venue in the fundamental understanding of the physics of anisotropic granulates and the subtle interplays between particle shape and inelasticity.

Acknowledgments

References

[1] Aranson I S and Tsimring L S, 2006 *Rev. Mod. Phys.* **78** 641
[2] Pöschel T and Schwager T, 2005 *Computational Granular Dynamics* (Berlin: Springer)
[3] Brey J J, Ruiz-Montero M J and Cubero D, 1996 *Phys. Rev.* E **54** 3664
[4] Garzó V and Dufty J, 1999 *Phys. Rev.* E **60** 5706
[5] Brey J J, de Soria M I G, Maynar P and Ruiz-Montero M J, 2004 *Phys. Rev.* E **70** 011302
[6] Haff P K, 1983 *J. Fluid Mech.* **134** 401
[7] Maass C C, Isert N, Maret G and Aegerter C M, 2008 *Phys. Rev. Lett.* **100** 248001
[8] Miller S and Luding S, 2004 *Phys. Rev.* E **69** 031305
[9] Nie X, Ben-Naim E and Chen S, 2002 *Phys. Rev. Lett.* **89** 204301
[10] Puglisi A, Loreto V, Marconi U M B, Petri A and Vulpiani A, 1998 *Phys. Rev. Lett.* **81** 3848
[11] Luding S and Herrmann H J, 1999 *Chaos: Interdiscip. J. Nonlinear Sci.* **9** 673
[12] Luding S, Huthmann M, McNamara S and Zippelius A, 1998 *Phys. Rev.* E **58** 3416
[13] Goldhirsch I and Zanetti G, 1993 *Phys. Rev. Lett.* **70** 1619
[14] Schwager T, 2007 *Phys. Rev.* E **75** 051305
[15] Brilliantov N V and Pöschel T, 2000 *Phys. Rev.* E **61** 5573
[16] Shinde M, Das D and Rajesh R, 2009 *Phys. Rev.* E **79** 021303
[17] Brilliantov N V, Spahn F, Hertzsch J M and Pöschel T, 1996 *Phys. Rev.* E **53** 5382
[18] Luding S, 1998 *Physics of Dry Granular Media* (*NATO ASI Series E* vol 350) ed H J Herrmann, J-P Hovi and S Luding (Dordrecht: Kluwer Academic) pp 285–304
[19] Luding S, Clément E, Blumen A, Rajchenbach J and Duran J, 1994 *Phys. Rev.* E **50** 4113
[20] Bodrova A and Brilliantov N, 2009 *Physica* A **388** 3315
[21] Brilliantov N, Salueña C, Schwager T and Pöschel T, 2004 *Phys. Rev. Lett.* **93** 134301
[22] Huthmann M and Zippelius A, 1997 *Phys. Rev.* E **56** R6275
[23] Brilliantov N V, Pöschel T, Kranz W T and Zippelius A, 2007 *Phys. Rev. Lett.* **98** 128001
[24] Ulrich S, Aspelmeier T, Zippelius A, Roeller K, Fingerle A and Herminghaus S, 2009 *Phys. Rev.* E **80** 031306
[25] Cafiero R, Luding S and Herrman H.J, 2000 *Phys. Rev. Lett.* **84** 6014
[26] Cafiero R, Luding S and Herrman H J, 2002 *Europhys. Lett.* **60** 854
[27] Aspelmeier T, Giese G and Zippelius A, 1998 *Phys. Rev.* E **57** 857
[28] Affouard F, Kröger M and Hess S, 1996 *Phys. Rev.* E **54** 5178
[29] Villarruel F X, Lauderdale B E, Mueth D M and Jaeger H M, 2000 *Phys. Rev.* E **61** 6914
[30] Wouterse A, Luding S and Philipse A P, 2009 *Granular Matter* **11** 169
[31] Azéma E, Radjai F and Saussine G, 2009 *Mech. Mater.* **41** 729
[32] Hidalgo R C, Zuriguel I, Maza D and Pagonabarraga I, 2009 *Phys. Rev. Lett.* **103** 118001
[33] Alonso-Marroquin F, 2009 *Europhys. Lett.* **83** 14001
[34] Kudrolli A, Lumay G, Volfson D and Tsimring L S, 2008 *Phys. Rev. Lett.* **100** 058001
[35] Peruani F, Deutsch A and Bär M, 2006 *Phys. Rev.* E **74** 030904
[36] Helbing D, 2001 *Rev. Mod. Phys.* **73** 1067
[37] Ben-Jacob E, Cohen I and Levine H, 2000 *Adv. Phys.* **49** 395
[38] Tillemans H-J and Herrmann H J, 1995 *Physica* A **217** 261
[39] Kun F and Herrmann H J, 1996 *Comput. Methods Appl. Mech. Eng.* **138** 3
[40] Kun F and Herrmann H J, 1999 *Phys. Rev.* E **59** 2623

[41] Alonso-Marroquín F, Vardoulakis I, Herrmann H J, Weatherley D and Mora P, 2006 *Phys. Rev.* E
      74 031306
[42] Pena A A, Lind P G, McNamara S and Herrmann H J, 2007 arXiv:0709.3716
[43] Cundall P and Strack O, 1979 *Geotechnique* **29** 47
[44] Allen M P and Tildesley D J, 1987 *Computer Simulation of Liquids* (Oxford: Clarendon)
[45] Brilliantov N V and Poschel T, 2000 *Phil. Trans.: Math. Phys. Eng. Sci.* **360** 415
[46] van Noije T P C, Ernst M H, Trizac E and Pagonabarraga I, 1999 *Phys. Rev.* E **59** 4326
      Pagonabarraga I, Trizac E, van Noije T P C and Ernst M H, 2001 *Phys. Rev.* E **65** 022303